Acta Materialia 188 (2020) 623–634

Contents lists available at ScienceDirect

Acta Materialia

journal homepage: www.elsevier.com/locate/actamat

Full length article

Interface facilitated transformation of voids directly into stacking fault tetrahedra

X.F. Kong[a,b,1], N. Gao[c,d,1], I.J. Beyerlein[e], B.N. Yao[a,b,f], S.J. Zheng[g,h,*], X.L. Ma[g], D. Legut[i,j], T.C. Germann[k], H.J. Zhang[l,m], R.F. Zhang[a,b,**]

[a] School of Material Science and Engineering, Beihang University, Beijing 100191, PR China
[b] Center for Integrated Computational Materials Engineering, International Research Institute for Multidisciplinary Science, Beihang University, Beijing 100191, PR China
[c] Institute of Frontier and Interdisciplinary Science and Key Laboratory of Particle Physics and Particle Irradiation (MOE), Shandong University, Qingdao 266237, PR China
[d] Institute of Modern Physics, Chinese Academy Sciences, Lanzhou 730000, PR China
[e] Mechanical Engineering Department, Materials Department, University of California at Santa Barbara, Santa Barbara 93106, United States
[f] Shen Yuan Honors College, Beihang University, Beijing 100191, PR China
[g] Shenyang National Laboratory for Materials Science, Institute of Metal Research, Chinese Academy of Sciences, Shenyang 110016, PR China
[h] Tianjin Key Laboratory of Materials Laminating Fabrication and Interface Control Technology, School of Materials Science and Engineering, Hebei University of Technology, Tianjin 300130, PR China
[i] IT4Innovations, VSB-Technical University of Ostrava, CZ 70800 Ostrava, Czech Republic
[j] Nanotechnology Center, VSB-Technical University of Ostrava, CZ 70800 Ostrava, Czech Republic
[k] Theoretical Division, Los Alamos National Laboratory, Santa Fe, NM 87545, United States
[l] National United Engineering Laboratory for Biomedical Material Modification, Dezhou 251100, PR China
[m] Department of Vascular & Intervention, Tenth Peoples' Hospital of Tongji University, Shanghai 200072, PR China

ARTICLE INFO

Article History:
Received 11 November 2019
Revised 20 January 2020
Accepted 17 February 2020
Available online 21 February 2020

Keywords:
Voids
Stacking fault tetrahedron
Interface
Transformation
Dislocation
Damage

ABSTRACT

Voids, helium bubbles and stacking fault tetrahedra (SFTs) are common irradiation-induced defects in face-centered cubic (FCC) metals and their alloys that have detrimental effects on their deformation behavior and lifetime. The formation mechanisms of voids and SFTs have been investigated in single crystals but the potential augmentation of these mechanisms by a heterophase interface has not been well studied. Here, using transmission electron microscopy (TEM), we report on the stability of both SFTs and voids at interfaces in an irradiated Cu/Ag nanolayered composite. With atomistic simulations, we show that the heterophase interface can promote the transformation of voids (<2 nm diameter) directly into SFTs. The interfacial misfit dislocations generate an atomically varying stress field that substantially reduces the activation barrier for the transformation at an interface compared to that in a single crystal or coherent interface. The transformation mechanism involves the sequential hopping of vacancies, starting at the interface and then later progressing to the nearest and next nearest atomic layers. The calculations further show that just a few helium atoms can hinder this mechanism and stabilize interfacial voids, explaining the coexistence of voids and SFTs near the interface observed experimentally. Last, the effect of stabilized defects at the interface on dislocation nucleation is studied via atomistic calculations employing quasi-static loading schemes. The results indicate that both voids and SFTs promote interfacial dislocation nucleation, which, in turn, damages the SFTs. These findings can provide the insight needed to design strategies for healing irradiation defects by interface engineering.

1. Introduction

High-energy particle irradiation can produce extremely high concentrations of crystalline defects, such as bubbles, voids, dislocation loops and stacking fault tetrahedra (SFTs) in face-centered cubic (FCC) metallic materials, such as Ag, Cu, Ni and stainless steel [1–5]. While these defects are nanoscale in dimension, their concentrations are still an order of magnitude greater than those expected under thermodynamic equilibrium states. The formation of these irradiation-induced defects contributes to the degradation in the mechanical properties of irradiated materials, such as embrittlement, loss of ductility, and irradiation hardening [6–9]. These detrimental changes can be traced to their interactions with dislocations, which glide in order to accommodate mechanical deformation. Studies of these interactions by atomic-scale simulations

* Corresponding author at: Shenyang National Laboratory for Materials Science, Institute of Metal Research, Chinese Academy of Sciences, Shenyang 110016, PR China.
** Corresponding author at: School of Material Science and Engineering, Beihang University, Beijing 100191, PR China.
E-mail addresses: sjzheng@imr.ac.cn (S.J. Zheng), zrf@buaa.edu.cn (R.F. Zhang).
[1] These authors contributed equally to this work.

https://doi.org/10.1016/j.actamat.2020.02.044
1359-6454/

have reported that voids/He-bubbles are harder to shear by dislocation glide than SFTs and thereby pose the greater barrier to slip [10–13]. Furthermore, while gliding dislocations negligibly affect the size of the void, they may split or even annihilate the SFT [14–20]. For these reasons, the relative amounts of voids vs. SFTs in a material are expected to greatly affect the structural properties of irradiated metals [21].

A process that affects this ratio is the transformation of voids into SFTs. Several studies have been devoted to understanding the mechanism underlying the transformation, in which the formation of Frank loops is explored as a key step for such transformations [22–24]. This mechanism indicates that the vacancies should first aggregate into a vacancy plate, which can then collapse to form a Frank dislocation loop. Afterward an SFT is generated by the movements of Shockley partial dislocations that dissociated from the Frank dislocation loop. Recent work by Uberuaga et al. [25] demonstrated that voids in a single Cu crystal can directly transform into SFT, by a different mechanism not involving an intermediate formation of a Frank loop. In that mechanism, vacancy jumps were demonstrated to play an important role in the formation of SFT. As a vacancy executes a hop, the corresponding movable Cu atom enters the void, triggering the transformation event.

The aforementioned studies only focused on transformation phenomena in single crystals, while the effects of grain boundaries, interfaces or surfaces, on the transformation have not been considered. One common remedy to manage irradiation defects is by introducing a high density of bi-phase interfaces [5,26–32]. Joining two dissimilar crystal structures, these interfaces are comprised of dislocations, some of which are intrinsic to the interface, called misfit dislocations, to accommodate the mismatch in lattice parameter. Several studies involving molecular dynamic (MD) simulations have observed that these interfacial dislocations influence the ability of the interface to annihilate irradiation defects like vacancies, interstitials [30–32]. Nevertheless, apart from studies on the trapping of point defects at bi-phase interfaces, similar atomic-scale studies on the transformations of voids and SFTs at interfaces have yet to be carried out.

In this work, using transmission electron microscopy (TEM) analysis and atomistic simulations, we investigate the transformation between voids and SFTs at Cu/Ag interfaces. We show that semi-coherent interfaces can promote the transformation of voids into SFTs. The interfacial misfit dislocations, which are inherent to these interfaces, generate a periodically varying stress field that can promote the transformation of a nearby void into an SFT via a mechanism that is different from any previously suggested transformation mechanisms in single crystals [23–25,33–35]. This local interface stress-assisted mechanism has a much lower activation energy barrier than the transformation mechanisms prevailing in bulk crystals and also at coherent interfaces. The mechanism entails the initiation of vacancy hopping where a void meets a fluctuating high stress at the interface, followed by an aggregation process to a tiny four-atom-SFT-unit. The interface stresses found to trigger this mechanism are not exceptionally high stress concentrators, suggesting that the process is not a particularly rare occurrence. To investigate the influence of voids and SFTs on interface-facilitated plasticity, we perform quasi-static and dynamic atomistic calculations under various loading conditions. The results show that both voids and SFTs lower the barrier for dislocation nucleation from interfaces and the SFTs can be removed from the interface by the freshly emitted dislocation.

2. Methodology

2.1. Materials fabrication, characterization and irradiation

The Cu/Ag multilayered samples were prepared through a flux-melting technique [36] with an average layer thickness of approximately 45 nm for Cu and 85 nm for Ag, corresponding to the eutectic composition of Cu and Ag (40Cu–60Ag at.%). This fabrication process has been shown previously to produce low energy, semi-coherent interfaces [36].

From this sample, TEM foils were prepared by a conventional cross-sectioning method, consisting of low-speed saw cutting, mechanical polishing, dimpling, and ion milling on a Gatan precision ion polishing system (PIPS). TEM analyses were performed on a Cs-corrected Titan 80-300 (FEI) operated at 300 kV. He implantation was conducted on the Cu/Ag TEM foils at 450 °C with 200 keV He-ions up to a fluence of 2×10^{17} ions/cm^2.

2.2. MD simulations and analyses

The atomistic simulations are performed using LAMMPS [37] and employing interatomic potentials for Cu [38], Ag [39] and Cu-Ag [39], derived from the embedded atom method (EAM). Pair potentials for modeling the Cu-He, Ag-He and He-He interactions are selected based on the ability to reflect a strong repulsive interaction at short distances [40,41].

Based on the HR-TEM observation of the earlier work [42], interface models used to investigate the transformation process are created and assembled from two perfect crystals with a specific orientation relation *x*-axis along ⟨112⟩, *y*-axis along ⟨111⟩ and *z*-axis along ⟨110⟩, as shown in Fig. S1 in the Supplementary Material (SM). Both commonly observed types of {111} interfaces are considered, one with a cube-on-cube and another with a twin/matrix orientation relationship, and both give nearly the same results in the void-to-SFT transformation studies to follow. The dimensions of the interface models are chosen to be 11.5 nm × 14.2 nm × 11.0 nm in the *x, y, z* directions, respectively. The dimensions in the *x* and *z* directions are not arbitrarily chosen because of the incommensurate nature of the lattice constants between Ag and Cu. They are instead determined such that the strains imposed on Ag and Cu layers are minimized [43], to ensure periodic boundary conditions, and to create a void in Wulff construction, consisting of only {111} and {100} crystal planes. Periodic boundary conditions are applied in the three directions of the simulation box. The simulations are performed with the timestep of 1 fs (0.001 ps) under the isobaric-isothermal (NPT) ensemble and zero stresses are enforced in all three directions. The temperature of the simulation cell is elevated in increments of 50 K. At each temperature, the system is annealed for 10 ns to detect whether the transformation occurs or not. If not, the temperature is increased by 50 K and another annealing step is performed for another 10 ns. We repeat above process until the transformation occurs and its associated temperature determined. We elevated the temperature directly rather than continuously in order to minimize the effect of heating rates on the transformation mechanism and help to isolate the role interfaces played in the transformation. Once the transformation temperature is determined, simulations are repeated to check the repeatability of the transformation mechanism. At each temperature level below the transformation temperature, the annealing time is reduced to 40 ps. At the target transformation temperature, the annealing time is 10 ns.

Interface models with dimensions of 15 nm × 30 nm × 13 nm, were built to investigate the mechanisms of dislocation nucleation. An athermal, quasi-static loading scheme was first adopted, and therefore the temperature effect is removed since we are focusing on a nucleation mechanism that depends solely on complex potential energy landscape of atomic configuration. The relaxation schemes and loading schemes we employed for all interface models in this work follow those already detailed in [44–46], and thus, only a relatively brief description is given below. To obtain a model of an interface at equilibrium, the first step involves dynamically adjusting the in-plane x and z dimensions, while simultaneously applying a displacement gradient along y. The atomic forces in the cell are then relaxed using fast inertial relaxation engine (FIRE) dynamics and conjugate gradient (CG) minimization. Finally, the internal stresses that satisfy the condition $\sigma_{xx}^{Cu} + \sigma_{xx}^{Ag} = 0$, $\sigma_{zz}^{Cu} + \sigma_{zz}^{Ag} = 0$, $\sigma_{yy}^{Cu} = \sigma_{yy}^{Ag} = 0$, are calculated. To subsequently induce the dislocation to nucleate, the relaxed interface model is uniformly strained in increments of 0.1% along one of the three orthogonal

directions. At each increment, the relaxation process is repeated in order to achieve the desired uniaxial stress state. For example, when tension loading is applied along the x-axis, the relaxation step ensures that $\sigma_{yy}^{Cu} = \sigma_{yy}^{Ag} = 0, \sigma_{zz}^{Cu} + \sigma_{zz}^{Ag} = 0$, and $\sigma_{xx} = (\sigma_{xx}^{Cu} + \sigma_{xx}^{Ag})/2$.

In order to evaluate the effect of He atoms and temperature on the deformation mechanisms, simulations of continuous loading were also performed. Due to the lack of recoil atoms in radiation, the total He concentration in the implanted TEM foils is rather low [47]. Hence He concentrations of 0.05 atom percent and 0.1 atom percent were considered. Interface models used here were the same as that in quasi-static simulations. Periodic boundary conditions were imposed and again, the stresses were kept at zero in all three directions by using the NPT ensemble. He atoms were randomly introduced to the octahedral interstices of models. Similar with the previous study [48], the models were equilibrated at 600 K for 800 ps to reach the steady state of the systems. The temperature was then decreased to 300 K for a time period of 15 ps and annealed for 5 ps. After preparation of the He-interface systems, uniaxial deformations were conducted at a strain rate of 10^8 s^{-1} to a strain of 10%.

Atomic configurations in both unstressed and stressed interfaces are visualized using the OVITO [49] and VESTA [50] software. The dislocation extraction algorithm (DXA) [51] and Nye's tensor analysis (NTA) [52,53] are used to locate and quantify the dislocations. The DXA method, already embedded in OVITO, can identify a wide range of dislocation types and extract dislocation lines. The NTA analysis can identify dislocations without a need to construct the Burgers circuit [52,53], unlike the DXA method. In a defective region, the vector dr' is related to it's dr in the perfect crystal by the local deformation tensor G:

$$dr = dr' \cdot G \tag{1}$$

The closed Burgers circuit C' in the dislocated crystal consisting of lattice vectors satisfies $0 = \sum_{C'} dr'$. Transforming these vectors into their images will result in an unclosed path C, which defines the Burgers vector b:

$$b = -\sum_{C} dr = -\sum_{C'} dr' \cdot G \tag{2}$$

Replacing the summation in Eq. (2) by an integral and then applying Stokes' theorem gives the following transformation:

$$b = -\oint_{C'} dr' \cdot G = -\iint_{A} n \cdot (\nabla \times G) \tag{3}$$

The Nye tensor is defined by describing the distribution of the infinitesimal dislocations [54], according to

$$db = n \cdot a dA \tag{4}$$

Comparing Eqs. (3) and (4), we finally obtain the expression:

$$a = -\nabla \times G \tag{5}$$

To overcome any difficulty in obtaining the Burgers vectors by an integral, Dai et al. [55] proposed a simple scheme to resolve the dislocation distributions via single value decomposition of the Nye tensor. As will be shown, the decomposition of the Nye tensor is an extension of the Nye tensor, which provides a convenient way to determine the Burgers vector and line sense [54]:

$$a = \sum_{\xi=1}^{3} \sigma_{\xi} u_{\xi} v_{\xi} \tag{6}$$

Consider for instance $n = u_1$. Combining Eqs. (4) and (6) for this case, we obtain:

$$db = n \cdot a dA = u_1 \cdot \sigma_1 u_1 v_1 dA = \sigma_1 v_1 dA \tag{7}$$

In Eq. (7), the line sense and Burgers vector can be identified as u_1 and v_1 respectively, while the density of dislocations can be determined by σ_1.

In Eq. (5), the parameter G can be calculated by a linear least-square fit as [52,53]:

$$G = Q^{+}P \tag{8}$$

where $Q(\gamma)$ $(\gamma = 1, 2, \ldots, \lambda)$ is the radius vectors of the neighbors in the dislocated configuration and $P(\gamma)$ corresponds to the reference vector. The integer value of λ gives the number of neighbors that are considered. The matrix $Q^{+} = (Q^{T}Q)^{-1}Q^{T}$ is the Penrose-Moore inverse of Q, where superscripts T and -1 signify the transpose and inverse of the matrix, respectively.

3. Results

3.1. Microscopic view of the irradiated Cu/Ag sample

He-implantation was first conducted on the TEM foil of the Cu/Ag nanolayered composite. After irradiation, both voids and SFTs have formed in the Ag lamellae. As we can see in Fig. 1a, voids prefer to be near or at the interface, while SFTs prefer to form within the Ag lamellae. The void sizes range from 5 nm to 11 nm, and the SFT sizes range from 3 nm to 9 nm. However, we also observe the coexistence of voids and SFTs at the interface, as shown in Fig. 1b. Closer examination in Fig. 1c, d shows the existence of the SFT at the interface and the void within the Ag lamella. As we can see, voids are faceted and have an octahedron shape, which is the same as that observed in previous studies [42,47]. This shape follows that predicted by the Wulff construction to minimize surface free energy [42]. Evidently, under high-energy He implantation, both vacancy type defect clusters, voids and SFTs, develop at the Cu/Ag interface. However, in the case of coarse-grained, single-phase metals, nearly all defects after He-ions irradiation are voids and bubbles [56,57]. The present observations motivate questions regarding the effect of interfaces on the stability of void and SFTs, such as, which one is more stable at the interface, and does the interface favor voids or SFT formation? Furthermore, bearing in mind that interfaces can govern plastic deformation mechanisms by serving as sources or preferred sites for lattice dislocation [44–46,58], interfacial voids or SFTs can potentially augment dislocation/interface interactions.

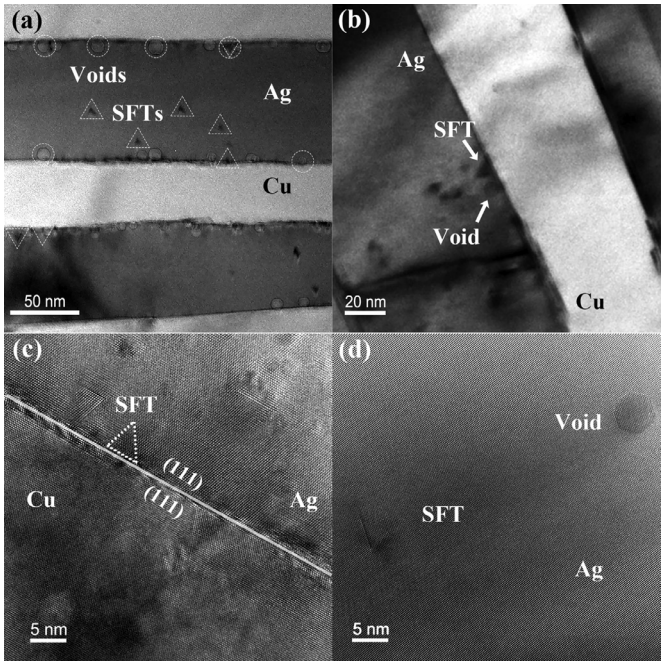

Fig. 1. Cu/Ag multilayered sample after He irradiation. (a) Under-focus (−0.5 μm) TEM image of the distribution of voids and STFs. (b) Over-focus (+0.5 μm) TEM image of STF and void in the interface at an. (c) HR-TEM image of the SFT at the Ag side interface. (d) HR-TEM image of the void and the SFT in the Ag layer.

3.2. Equilibrium interface structure with a void

To study the stability of voids at the interface, MD simulations were carried out on a model of a semi-coherent Cu/Ag interface and a nearby void, which has preferentially nucleated at the misfit dislocation intersections (MDIs) [59,60]. According to the TEM observations, we first considered a void in the shape dictated by the Wulff construction. The void is approximately 1.4 nm in diameter (containing 38 vacancies) and is introduced to the Ag-side of the Cu/Ag interface (see Fig. S2 in the SM). At this length scale, this construction only requires that the void surfaces consist of {111} and {100} crystal planes. Voids of this scale were directly observed in the He-implanted Cu/Ag nanolayered composites at 400 °C in Ref. [47], see Fig. S3 in the SM. It should be noted that Fig. S3 shows many voids within the Cu layer, contrary to Fig. 1. This is because the energy of the He ions in our present study is lower than that in Ref. [47], while the irradiation temperature is higher than that in Ref. [47]. Thus, in our study, while less vacancies are generated, they have higher mobility. Consequently, the "pump effect" as described in Ref. [47] becomes more effective. The Cu vacancies are driven to transmit across the interface into the interior of Ag layers rather than remaining in the Cu side. In Fig. 1 in our study, no voids are detected in the Cu layer.

Fig. 2 provides a spatial mapping of the defects present in the interface-void system. For the semi-coherent interface, the distribution and edge character of the misfit dislocation network can be seen using the DXA [51] and NTA [52–54]. Both methods expose the regions of perfect FCC stacking and faulted hexagonal close-packed (HCP) stacking and the edge-type partial dislocations that separate them, as seen in Fig. 2a and b. The local region, where the void contacts the Ag side of the interface, is also the free surface and there is no Ag atom (marked in Fig. 2a by the dashed hexagon). Fig. 2c presents the atomic shear stress distribution at the interface after annealed at 300 K and then minimized. Away from the void, we observe that the positive and negative shear stresses (τ_{yx} and τ_{yz}) are distributed alternatively and periodically in the interface, with the peak stress and potential energy concentrations generated at the MDIs. Comparison with the structure and stress distribution of the void-free interface, shown in Fig. S4 in the SM, finds a similar structure and stress distribution. Thus, this variation results solely from the intrinsic misfit dislocation array of the semi-coherent interface and not that of the nearby void. Near the void, however, the stress and energy potential become noticeably disrupted. In particular, when the void lies in the vicinity of the MDIs, the atoms possess higher excess potential energy (EPE) and the shear stress distribution becomes highly heterogeneous. The misfit dislocation network breaks down sharply at the surface of the void. From the EPE map shown in Fig. 2d, atoms with the higher potential energy are not located at the vertex in the core of the misfit dislocations. Instead, the high EPE atoms lie at regions between these vertex points (see the atoms labeled by symbols of *a, b, c* in Fig. 2d). The atomic layers shown in Fig. 2 are the Ag1st and Cu1st layers, where 1st means the layer immediately adjacent to the interface. These are also the layers with the largest perturbations and highest stresses generated by the misfit dislocations. For the Ag2nd, Ag3rd and Ag4th... layers further away, the perturbations and stresses diminish. This is consistent with the transformation process below, in

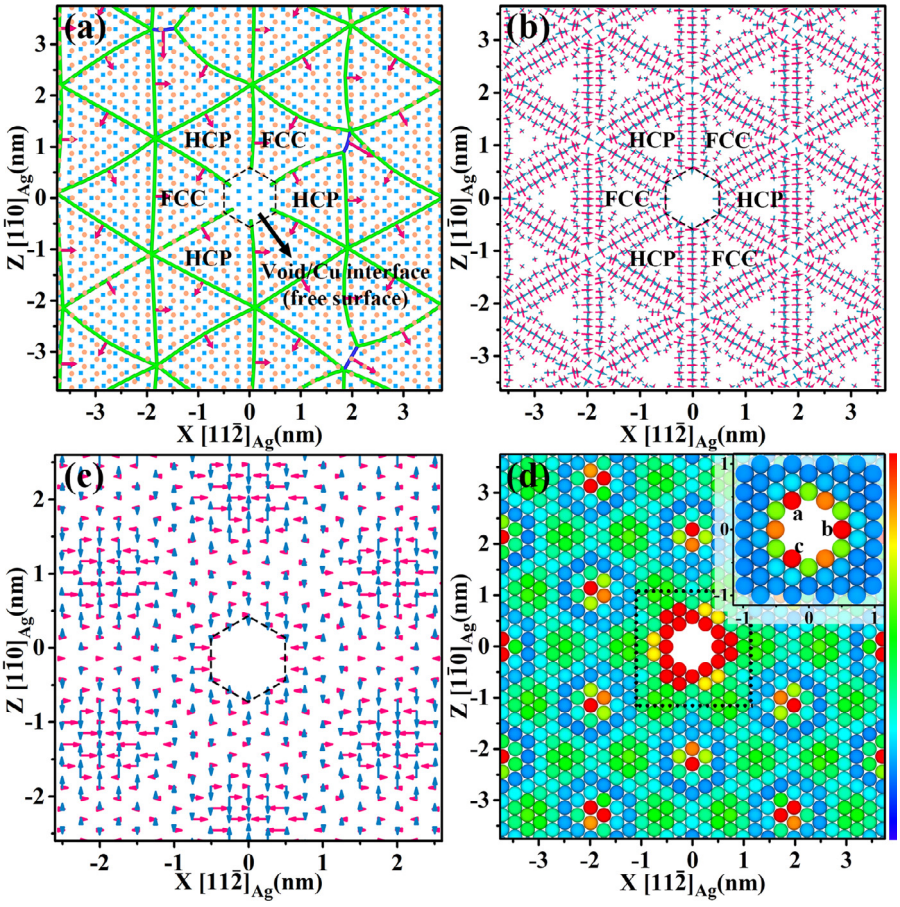

Fig. 2. The misfit dislocation, shear stress and energy distributions of the void-containing Cu/Ag interface. (a) Misfit dislocation lines (green lines) and Burgers vectors (red arrows) calculated by DXA. The orange circles indicate Ag atoms and the blue squares indicate Cu atoms. (b) Nye tensor plots from the Ag side of the interface. The red and blue arrows indicate the Burgers vectors and dislocation lines, respectively. (c) Shear stress distributions from the Ag side of the interface. The pink arrows indicate τ_{yx} and the blue arrows indicate τ_{yz}. The length of each arrow specify the magnitude of stress. (d) Energy distribution on the Ag side of the interface. The atoms are colored according to the excess potential energy, and red (or blue) color indicates relatively high (or low) energy. The inset adopts the same color bar but uses a different scale. (For interpretation of the references to color in this figure legend, the reader is referred to the web version of this article.)

which the atoms with the highest excess potential energy in the Ag1st layer are the first to hop.

3.3. Transformation process at the interface

To this interface/void assembly, the temperature is increased in 50 K increments and at each increment, annealed to equilibrate the structure, until the final temperature of 850 K is reached. Below 700 K, the atoms vibrate around their equilibrium positions. Some atoms may begin to jump, but then they usually jump back to the original sites or exchange positions with other atoms. Approaching 800 K, the void to SFT transformation process occurs during the annealing, but at an extreme low rate. At 850 K, the void directly transforms into an SFT, relatively quickly, within 2.4 ns. The temperature effect in combination with the stress effect on the transformation rate can be understood by using transition state theory [25]:

$$\boldsymbol{R} = \boldsymbol{R}_0 \exp\left[\frac{-\Delta \boldsymbol{E}(\sigma)}{k_B T}\right] \tag{9}$$

where R and R_0 are the transformation and intrinsic rates, respectively. In Eq. (9), the energy barrier $\Delta \boldsymbol{E}(\sigma)$ is described as a function of stress state σ but independent of temperature. From Eq. (9), it is clear that a higher temperature would increase the transformation rate from a void to an SFT. The importance of the stress dependence will be discussed next.

The kinetic process of the direct transformation at 850 K is depicted in Fig. 3. It is observed that vacancy hopping is initially triggered on the interface side of the void, resulting in the displacements of Ag atoms along ⟨110⟩ directions, as indicated by the green arrow in Fig. 3a. For the three atoms with higher EPE (see the atoms labeled by symbols of *a, b, c* in Fig. 2d), it is found that they have the same probability to initiate the first jump. The inhomogeneous distribution of atomic EPE at the MDI-void intersection promotes these high priority jumps. From Eq. (9), it can also be understood that the energy barrier for the first jump reduces at the interface-void intersection plane where the stress is the highest. Atoms in this area jump initially, leading to a series of additional atomic movements, as will be described below.

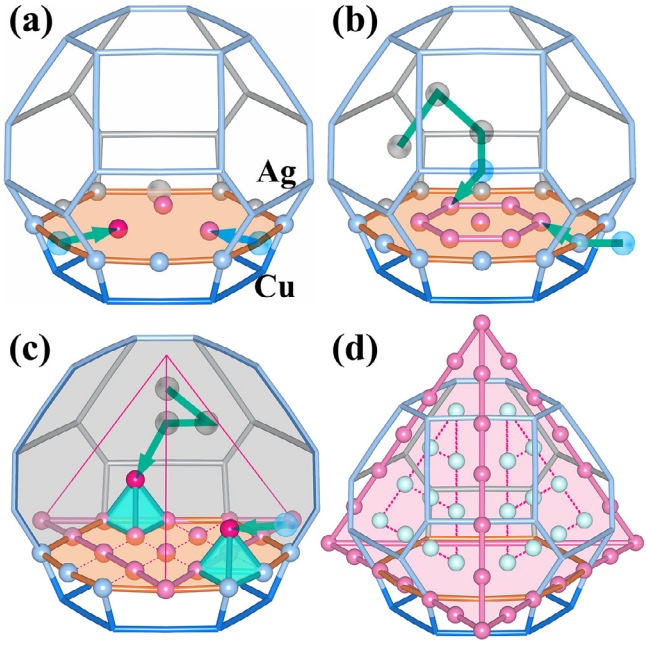

Fig. 3. Transformation process from a void to an SFT. Only the atoms belonging to the first Ag atomic layer of the interface and the atoms belonging to SFT are illustrated. Blue and gray shaded circles indicate the atomic positions in the front and back of the void, respectively. (For interpretation of the references to color in this figure legend, the reader is referred to the web version of this article.)

When one atom with high EPE starts to jump, the other two atoms jump immediately afterward, as indicated by the blue arrows. After these first jumps, subsequent jumps of vacancies are observed from the interface Ag layer to nearest and next nearest adjacent atomic Ag layers (see Fig. 3b). These atomic jumps fill atomic positions in the bottom plane of the void. This hopping process finally results in the formation of one surface of the SFT located in the interface. From this surface, the SFT starts to grow as shown in Fig. 3c. SFT growth can potentially begin after the formation of a small four-atom-SFT-unit, meaning it has two atoms on each edge. Many such four-atom-SFT units are formed and destroyed by thermal disturbances, indicating it is the critical unit size at this temperature. Once a unit stabilizes, a fast growth process follows in accordance with nucleation theory [61]. Fig. 3d shows a full-grown SFT with seven atoms on each edge formed in the end of the process.

In order to select a representative case, the transformations into SFTs of voids of other shapes and sizes are also investigated. Both size and shape are found to influence the temperature and time needed to finish the transformation. For the same shape, the bigger the void (more vacancies), the weaker is the interface effect. Further, a bigger void needs a higher temperature or longer times to transform into an SFT. For the same size, different initial void shapes share the same basic two-stage transformation mechanism. First, atom/vacancy hopping (at the interfacial end of the void) triggers the transformation and second, the SFT grows via the formation of four-atom-SFT units. The shape, however, affects the transformation times, by primarily affecting the contact area between the void and the interface. This contact area directly determines the part of the void engaging in the interface, influencing both the number of atoms/vacancies to initiate the first jump to trigger the transformation and the energy barrier of the jump. With this last aspect it is important to note that the void shape has to be stable. While we did not simulate every possible void shape, based on these simulations, the void in the shape of a Wulff construction is the most stable one at a relatively low temperature. Examples of transformations of several other voids, are also provided in the Supplementary Material and Fig. S5.

Taking the above factors into consideration, we extend Eq. (9) for nucleation of SFT at the interface to:

$$\boldsymbol{R}_{void \rightarrow SFT} = N_{site} \rho \boldsymbol{R}_0 \exp\left[\frac{-\Delta \boldsymbol{E}(\sigma)}{k_B T}\right] \tag{10}$$

where N_{site} is the number of atoms that could initiate the first jump and ρ is probability of forming a stable four-atom-SFT-units, that is, not destroyed by thermal disturbances. As shown here, N_{site} and ρ are related to the area of the intersection area between the void and the interface as well as the size of the void, suggesting that the shape of the void would affect the transformation rate.

3.4. Transformation process in the Ag single crystal and the Ag twin interface

The foregoing direct void-to-SFT transformation mechanism in Cu/Ag interface is different from that reported earlier in the simulation of Cu [25]. As a second reference case, the simulation is repeated in a single Ag crystal to confirm that the transformation mechanisms seen in the interface still differ from those in the bulk. As shown in the left inset image of Fig. 4 (I and IV), the direct transformation from void to SFT is also observed in Ag but at a higher temperature, around 1050 K, than in the Cu/Ag interface. An interesting step that occurs early in the transformation process within the simulation of a single crystal Cu [25], which had used parallel-replica dynamics (PRD), involves a single hopping atom attracting another atom lying on the opposite side of the void surface. We find that this step also occurs in

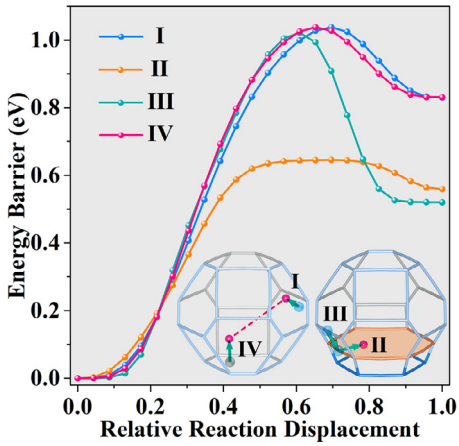

Fig. 4. Energy barrier for vacancy hopping. Processes I and IV are hopping processes in the void at the bulk Ag crystal. Processes II and III are hopping processes in the void at the Cu/Ag interface.

the Ag crystal, but over a much longer simulation time than in the Cu crystal. The difference in transformation time may be attributed to the different temperatures used in the studies; temperature can affect the probability and duration of the transformation. In contrast to both Cu and Ag, in the void-to-SFT transformation process at the Cu/Ag interface, the involvement of attracting atoms on opposite void surfaces is not observed, which is one of the many aspects.

To further elucidate the role of the misfit dislocations on the void-to-SFT transformation at the Cu/Ag interfaces, simulations are repeated for a void at a coherent $\Sigma 3\{111\}$ interface of Ag. Lacking misfit dislocations, the coherent interface develops a stress state at that is nearly homogeneous (see Fig. S6 in the SM). Some fluctuations in shear stress τ_{yx} and τ_{yz} are seen but these are orders of magnitude lower in value than the stress developing in the heterophase interface due to the misfit network. Consequently, a much higher temperature up to ~1000 K is required for the transformation from the coherent interface. These results would suggest the stress effect on energy barrier has the following relationship:

$$\Delta \boldsymbol{E}(\sigma) \sim \Delta \boldsymbol{E}(0) + \Pi \Omega \sigma \tag{11}$$

where Ω is the effective transformation volume and Π can be regarded as a constant related with the shear modulus. We note that the stress field generated in the crystals adjacent to the interface by the misfit dislocations contains both a hydrostatic component and deviatoric normal and shear stresses. A void or voids lying at the interface would only make this local interface stress field even more complex. Nonetheless, both the hydrostatic and deviatoric stresses are likely to play a role in the transformation, as will be discussed below in Discussion. Although it is an approximation, Eq. (11) embodies the dependence the energy barrier has on stress that we have identified in this study.

To calculate the activation barrier associated with the direct transformation from the void to SFT in the semi-coherent interface, we employ the nudge elastic band (NEB) [62] method. As seen in the results presented in Fig. 4, the calculated energy barrier for the initial jump of the Ag atom in the interface (Process II) along ⟨110⟩ direction is approximately 0.64 eV, which is a much lower value than the 1.04 eV for the void-to-SFT transformation in the Ag single crystal (Process I). It is also lower than the value (1.15 eV) reported for the transformation in a Cu single crystal under constant pressure [25]. The energy barriers for the subsequent jumps in the interface (Process III) are only slightly lower than the value (~1.04 eV) in Ag single crystal (Process IV). From Fig. 4, it is found that the jump associated with process II at the interface is triggered by the non-uniform stress at the interface and occurs at a much lower energy barrier. The migration energy barriers of a single point defect under different stress components have also been investigated previously [63–65]. It is found that the energy barrier varies with the vacancy migration direction and for a given stress condition (or stress state), the migration energy barrier of a vacancy decreases along a specific migration direction. The migration might be retarded by another stress state or another migration direction. These reductions in the vacancy migration energy were observed in tension, compression and shearing stress states respectively. Although the stress state may be less complex than that in the present situation, in which the effect of the voids (especially their shape and size) on the local stress distribution is also coupled with the heterogeneous stress field generated by misfit dislocations. But by affecting vacancy hopping (migration)—the basic unit procedure of the transformation process—the effect of stress field generated by the interface on the vacancy migration energy could be similar to the simple case.

3.5. Effect of He atoms on the transformation process

The foregoing barrier calculations support the finding that the interface can facilitate the transformation of a void into an SFT. While this would suggest voids are less likely to exist at interfaces, an irradiated Cu/Ag composite can still find both voids and SFTs at the Cu/Ag interface (see Fig. 1b). It is also possible that some He atoms could be trapped inside the void and SFT (see Fig. S7 and Fig. S8 in the SM) since the binding energy [66] between He and a vacancy cluster is positive. Because of the positive binding energy, the probability ρ and stress contribution $\Pi\Omega\sigma$ in Eqs. (10) and (11) would decrease and increase, respectively, indicating that voids and SFTs could coexist near the interface. To test this notion, MD simulations were performed to study the transformation of voids containing different concentrations of He atoms. Fig. 5a shows the average potential energy of the atoms belonging to the region affected by the void or the transformed SFT after annealing at 300 K and at 850 K and above. We find that He can stabilize the void, hindering its transformation. A relatively high temperature (up to 950 K) is needed for the transformation of a 38-vacancy void containing up to three He atoms. However, for the same void with more than three He atoms, the transformation does not occur, even at much higher temperatures of 1100 K. Such differences can be attributed to a repulsive interaction between the He and Ag atoms, which hinders the jumping of Ag atoms, resulting in an increase in $\Pi\Omega\sigma$ and hence reduction in ρ. Last, we considered an interface containing two voids, one with five He atoms and one without He atoms. They are placed in the interface at a distance of ~5 nm. The simulation temperature was increased to 1200 K in order to apply even higher thermal fluctuations to induce the possible transformation in both. Fig. 5b shows these cases after full relaxation. It is observed that the void without He atoms transforms into an SFT, while the void containing five He atoms does not. This finding provides further confirmation that He atoms stabilize voids against transformation.

3.6. The void and SFT facilitated dislocation nucleation at interface

In this section, we study the influence of voids and SFTs on the nucleation of dislocations. For the athermal, quasi-static deformation investigation, three cube-on-cube Cu(111)//(111)Ag interface models are built: 1) a void-free and SFT-free interface, 2) an interface containing a Wulff void, 1.4 nm in diameter, and 3) an interface containing a perfect SFT, comprised of 36 vacancies, and an edge length of 1.8 nm. Each interface model was relaxed using the procedures described earlier. To promote dislocation nucleation, the relaxed interfaces are deformed in uniaxial/biaxial tension and compression using schemes that mimic quasi-static deformation [44–46]. The strain was raised in increments of 0.1% until a dislocation was seen to nucleate from the interface and propagate into the crystal. The average stress in the system that was reached just before the dislocation appeared is deemed the critical stress. Table 1 summarizes the critical stresses for dislocation nucleation under compression or tension in

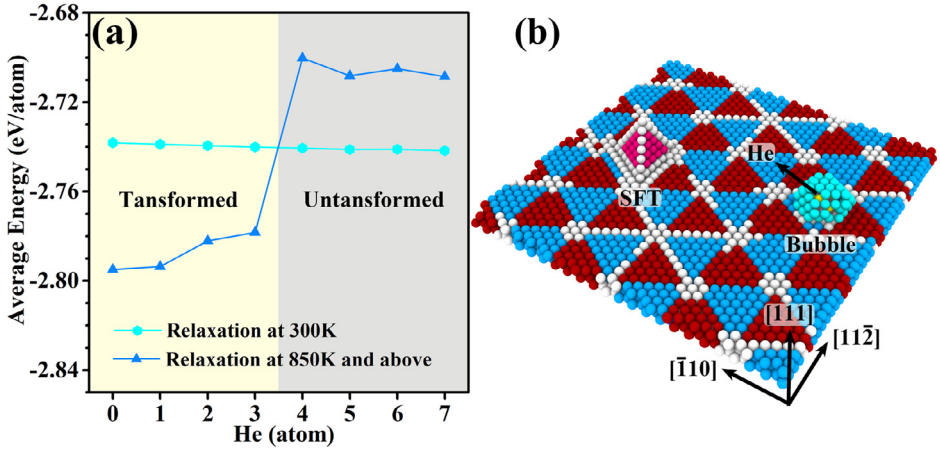

Fig. 5. Effect of He atoms on the void-to-SFT transformation. (a) Average potential energies of the atoms surrounding the void with He atoms or transformed SFT after annealed at a given temperature. (b) Co-existence of the SFT and 5He-void at the Ag side of the interface.

Table 1
Peak yield stresses before dislocation nucleation of the SFT-containing, the void-containing and the clean Cu/Ag interfaces. Results are given in GPa.

	Compression				Tension			
	x	*y*	*z*	*x-z*	*x*	*y*	*z*	*x-z*
SFT	**−3.67**	**−7.96**	**−8.78**	**−13.44**	5.40	9.63	**3.26**	**6.36**
Void	−4.84	−10.80	−10.24	−14.27	5.28	8.33	4.08	9.16
Clean	−7.43	−15.44	−12.27	−21.27	7.87	10.55	4.33	10.16

The bold values indicate that at these loading schemes, the cirtical stresses of the SFT-containing interface are lower than that of the void-containing interface.

one or two of the three axes (x, y, or z). In all cases, the void and SFT reduces the critical stress, and in most cases, the critical stresses of the SFT-containing interface are lower than those of the void-containing interface. The exception occurs under tension along the *x*-axis, wherein the critical stress decreases from 7.87 GPa for the pristine interface to 5.40 GPa for the SFT-containing interface and to 5.28 GPa for the void-containing interface. When the loading mode changes to compression, the critical stress becomes 7.43 GPa for the pristine interface, and dramatically lowers to 3.67 GPa for the SFT-containing interface and 4.84 GPa for the void-containing interface.

To identify the reasons for the influence of voids and SFTs on dislocation nucleation, the effective stress-strain curves and partial dislocation nucleation mechanisms under uniaxial loading are analyzed in Fig. 6, as well as in Fig. S9 in the SM. As the dislocation nucleates from the interface, we observe that the SFT undergo distinct shape changes and eventual removal, in a manner that depends on the direction and sense of loading. Under compression along the *x*-axis [11$\bar{2}$] or the *y*-axis [111], both the leading and trailing partials emit in succession from one face of the SFT, as shown in Fig. 6g and h, which completely removes it. As a consequence, the interface becomes atomically flat, as observed in Fig. 7. Biaxial tension in the x-z axes invokes a similar process, also eventually leading to the removal of the SFT (similar to Fig. 7b). Under tension along the *y* axis [111], however, three sets of leading partials nucleate from both the void- and SFT-containing interfaces. The SFT is absorbed, leaving a complex stacking fault junction at the interface, as shown in Fig. S9b in the SM. A similar situation occurs under biaxial x-z compression.

In contrast to the strong interactions that are seen to develop between the SFT and nucleated dislocations, the void is more stable. After dislocation nucleation, the void slightly changes its shape and hardly shrinks in size, as shown in Fig. 6d–f. Two factors are identified to contribute to the easier nucleation from the SFT-containing interface than the void-containing interface. First, compared to the void, the geometry of SFT generates severe stress concentrations in its vicinity. Such concentrations induce dislocations to nucleate. Fig. S10 shows the calculated Von Mises stress distribution of these two interfaces at equilibrium condition and at a compression strain of 3.0% along *x*-axis. It is clearly seen that the stress concentrations around the SFT are more severe than that around the void. Second, as a dislocation based defect, the SFT consists of stair-rod dislocations with Burgers vector of 1/6<110> along the edges of the tetrahedron. It is possible for the stair-rod dislocation to dissociate into two Shockley partial dislocations, i.e. $\beta\gamma \rightarrow \beta A + A\gamma$, that is 1/6[$\bar{1}$01] → 1/6[1$\bar{1}$2] + 1/6[$\bar{2}1\bar{1}$]. At equilibrium, this reaction would not occur because it is energetically unfavorable. However, under compression along *x*-axis, for instance, the Shockley partial βA in the ACD plane would be activated since it bears the maximum Schmid factor under this loading state [44]. After the stress enables the partial βA to nucleate, the partial, in turn, reacts with the SFT to damage it, as shown in Fig. 7a. When the interfaces are compressed along the *z* axis [1$\bar{1}$0] or stretched along *x* axis [11$\bar{2}$], leading Shockley partials nucleate from one side of void, again without a noticeable change in shape (see Fig. 6f and Fig. S9a in the SM). In contrast, two sets of leading partials nucleate from one edge of the SFT, leaving a small stable partial dislocation loop at one surface of the SFT, as shown in Fig. 6i and Fig. S9g in the SM.

In simulation, after introducing He atoms to the interface, equilibrating at 600 K and reducing the temperature to 300 K, significant lattice distortions are observed to develop. Frenkel pairs, He clusters and interstitial-induced dislocation loops form in both the Ag and Cu layers. As shown in Fig. S11 in the SM, the densities of these defects correlate positively with He concentration. In particular, the radii of the dislocation loops that developed in the interface with 0.1% He are larger than those that developed with 0.05% He. This difference is expected to have a significant influence on the subsequent deformation mechanism and the damage of the SFT. To test this notion, the system containing interfaces with two He concentrations was deformed in either uniaxial tension and compression. For interfaces with 0.05% He, dislocation nucleation occurs from the interfacial void or SFT and leads to the damage of the SFT, mechanisms similar to those seen in the case without He. None of the pre-existing dislocation loops activated prior to those forming from the void or SFT. Fig. 8 shows the stress–strain curves and dislocation nucleation mechanisms under compression along either *x*- or *y*-axis. As shown, for both the void- and SFT-containing interfaces, the pre-existing dislocation loop do not activate and rather new dislocations nucleate from the interfacial void or SFT. Under compression, the SFT is damaged by the just nucleated partial dislocation, similar to the process shown in Fig. 7, and the void hardly changes in shape. The deformation mechanisms in tension are also similar to those without He. In contrast, in the cases of interfaces with 0.1% He, plasticity is initiated by the activation of the dislocation loops, whose Burgers vectors are favorably oriented for glide, rather than dislocation nucleation from the void or SFT at the interface. Thus, the critical stress (the first drop in the strain–stress curve) is

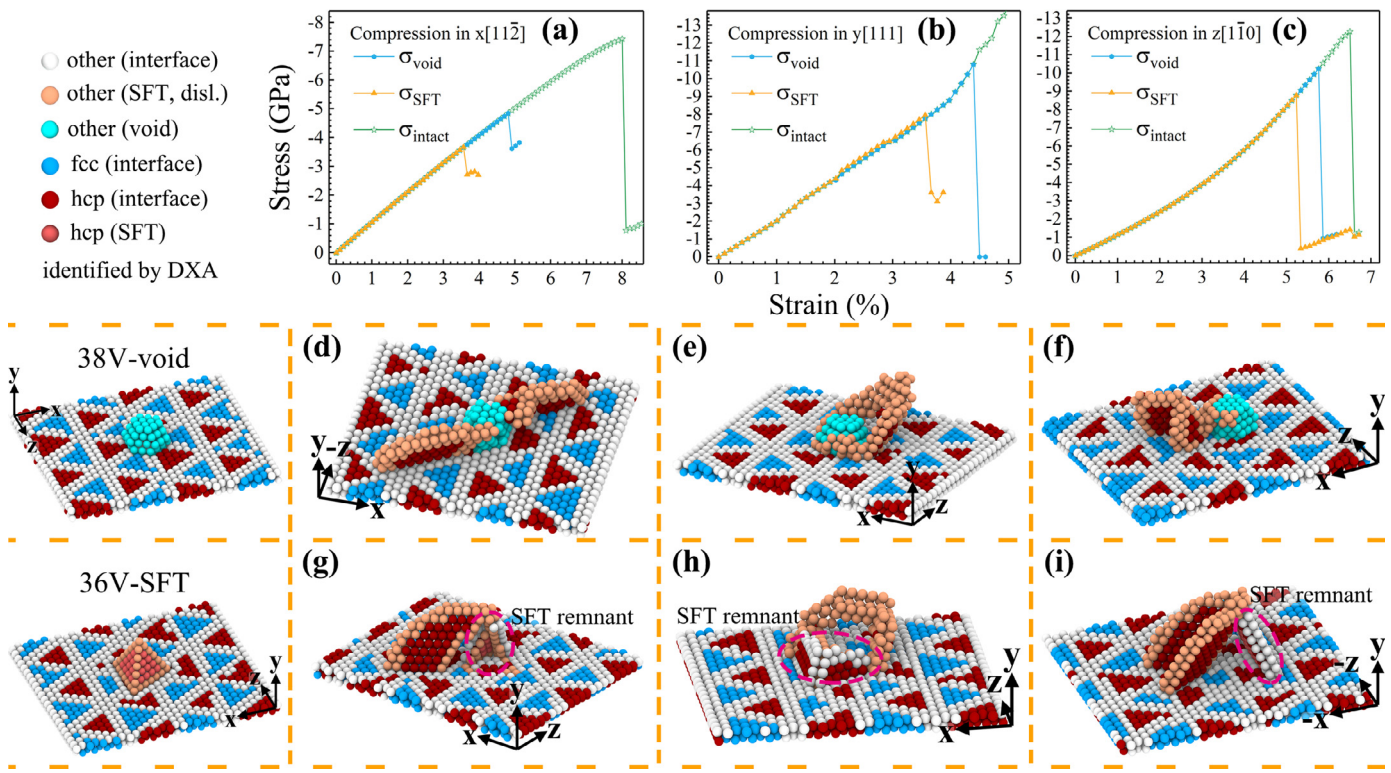

Fig. 6. (a)-(c) Effective stress–strain curves of the void-containing and SFT-containing interfaces under different compression loadings, and the corresponding dislocation nucleation mechanisms for (d)-(f) void-containing interfaces and (g)-(i) SFT-containing ones.

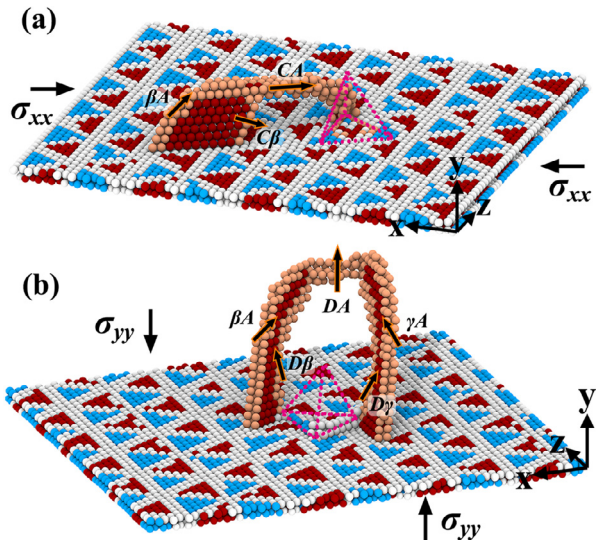

Fig. 7. The damage of an SFT through its reaction with a dislocation that has nucleated at the interface under (a) compression along the *x* axis [11$\bar{2}$] and (b) compression along the *y* axis [111].

determined by the orientations and types of dislocation loops induced by the He clusters. However, with further loading, the SFT becomes damaged by the subsequent dislocation nucleation, as shown in Fig. S12 in the SM. Thus, the damage mechanism of the SFT we proposed is also effective when He atoms are present at the interface.

Taken together, unlike in the case of a void, these findings indicate that dislocation nucleation is accompanied by the damage of the SFT defect at the interface, which would make dislocation nucleation more favorable from an SFT-containing interface than a void-containing interface. The SFTs are less stable against destruction than the voids at the heterophase interface.

4. Discussion

The results of this work identify two important interactions that bi-phase interfaces can have with irradiation defects, namely voids and SFTs, commonly occurring in FCC metals. The first pertains to the promotion of a void-to-SFT transformation, unlike that occurring within the crystal, and the second is an SFT-recovery mechanism that promotes dislocation nucleation from the interface. In both situations, the interface alters the defect density or the relative amounts of voids and SFTs maintained in the composite. In this way, interfaces can influence hardening of irradiated materials in an indirect way, when considering that voids and SFTs interact differently with moving dislocations [10,11,13,20].

Fig. 9a–c illustrates the different mechanisms for void-to-SFT transformations that have been studied for single crystals. None are like the interface-facilitated mechanism revealed in this work. Fig. 9a shows the vacancy plate-to-SFT process proposed for Cu, Ni and Al [24]. The plate first collapses to form a Frank dislocation loop, and then Shockley partial dislocations that dissociated from the Frank loop react to form the SFT. Fig. 9b depicts an alternative vacancy aggregation mechanism studied in Ni [35], in which a vacancy-tetrahedron cluster, resulting from the aggregation of randomly distributed vacancies, serve as a nucleation center of the SFT. In Fig. 9c, the direct transformation of a vacancy cluster into an SFT as seen in PRD simulations of Cu [25], is shown. In this event, the transformation takes place via a series of intermediate structural transformations that are enabled via vacancy/atom hops. The atom which initiates the first hop to start the transformation is determined by thermal fluctuations, and the atom executing the hop is selected without preference. The transformation mechanism from voids to SFTs at semi-coherent interfaces discussed in this work differs from these previously proposed ones. In the case of the interface-facilitated transformation, a dislocation reaction was not involved, the void does not morphologically change into a vacancy-tetrahedron cluster before transforming to an SFT, and the first vacancy jump is highly correlated with localized stress concentration regions in the interface. It

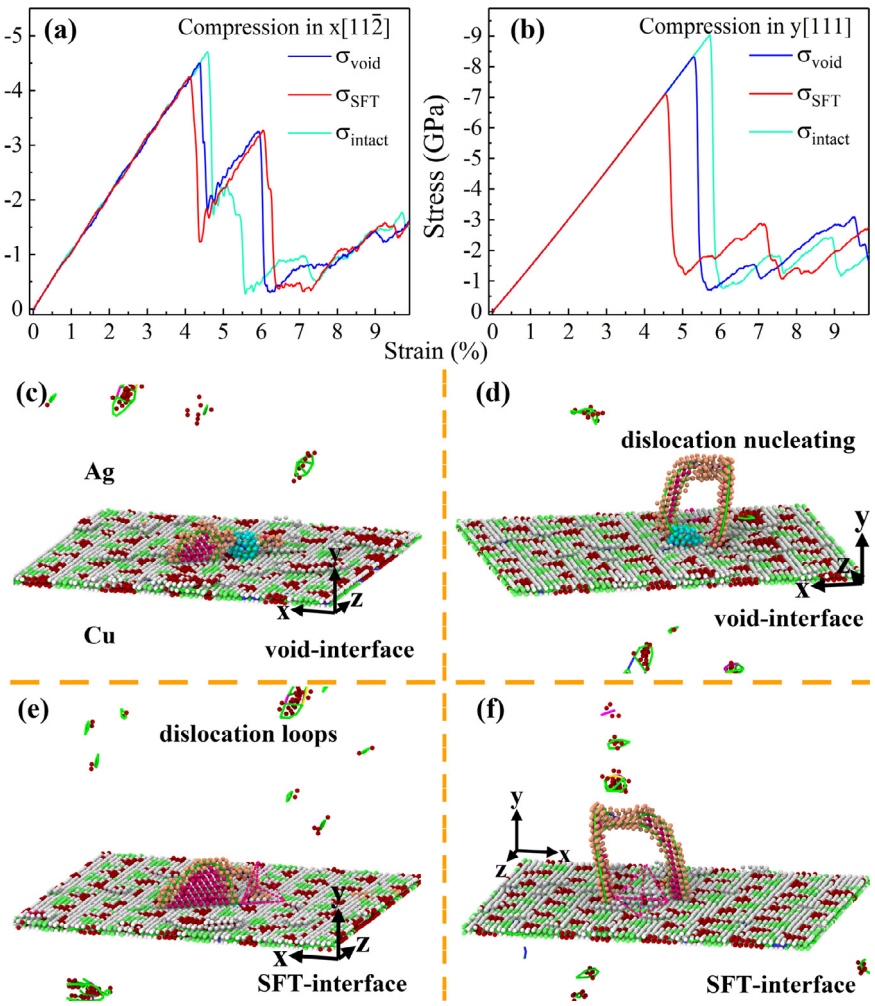

Fig. 8. (a)(b) Stress–strain curves of the void-containing and SFT-containing interfaces with 0.05% He under different compression loadings at 300 K, and the corresponding dislocation nucleation mechanisms for (c)(d) void-containing interfaces and (e)(f) SFT-containing ones.

should be noted that here we refer to the relative ease of the transformations directly from void to SFT (excluding the cases involving dislocations) with respect to two major indices, temperature and the number of He atoms. Regarding temperature, among all the Cu/Ag interface models, Ag twin models and single crystal Ag models in our work, the voids and annealing schemes are all the same. The results show that for the void at the Cu/Ag interface, only 850 K is required to accomplish the transformation into SFT, while for the void at the Ag twin boundary, the threshold temperature is approximately 1000 K. For the void in the single crystal Ag, a temperature of 1050 K is needed. Further, the energy barriers calculated by NEB method for vacancy hopping, which is the unit procedure to accomplish the transformation, suggest that the interface promotes vacancy hopping by reducing its barrier. With respect to the number of He atoms, our simulations show that the interface facilitates the transformation from the void to SFT, even when there are up to 3 He atoms in a 38-vacancy Wulff void at 950 K. But in the case of a void in a single crystal, at 1100 K, two or more He atoms can prevent the transformation. Hence, with no He or other noble gas, SFTs would dominate the interfaces. The findings in a more recent study by Han et al. [67] directly support our conclusions. In their study, a bulk Cu/Ag nanolayered sample was irradiated with 800 keV Ne-ions up to a fluence of 1.2×10^{16} ions/cm^2. According to the SRIM calculation, the region of radiation damage extends to a depth of 800 nm. At the depth of 900 nm from the sample surface, there is no cascade damage. But the irradiation-induced vacancies at the radiation damage zone could diffuse to such depth while Ne atoms could not, due to different mobilities between them. The TEM image shows that there are a large number of SFTs, rather than voids, lying at the Ag side interface, as given in Fig. S13 in the SM.

Here, we reveal a mechanism that damages even removing an SFT but not a void, when a stress is applied to the interface. When the dislocation first forms from the interface, it bows out as a half loop with a mixed character. We find that it can damage the SFT, particularly more efficiently than a void (Fig. 7). With the SFT removed, the interface then recovers its low energy state. This finding would imply that SFTs would be less stable than voids, especially under compressive tractions experienced at the interface. This finding is distinct from many studies that report that the intrinsic or constitutional defects of bi-metallic interfaces can trigger the formation of dislocations or SFTs in the adjoining crystal when under an applied load. Atomic-scale simulations in Ref. [44,68] have shown that the misfit dislocation intersections (MDIs) in the semi-coherent interface possess more free volume than the interior of the grain and these have been referred to as constitutional vacancies [29]. In simulation, it was found that dislocation nucleation from the interface reduced the excess volume at the MDIs [44,68], transporting the excess volume into the adjacent crystal. For Cu/Al interfaces under out-of-plane tension, Li et al. [69] observed in MD simulation, the development of a closed SFT on the Cu side and an open-ended SFT on the Al side. In this case, the SFTs formed via a dislocation reaction between Shockley partials that had emitted from the interface. Atomic-scale simulation of shock loading of Ni/Al interfaces in Ref. [70] reported the formation of stacking fault pyramids on the Al side. The square grid of the misfit dislocation network provides a template for forming the stacking fault pyramids. In all these cases, dislocations

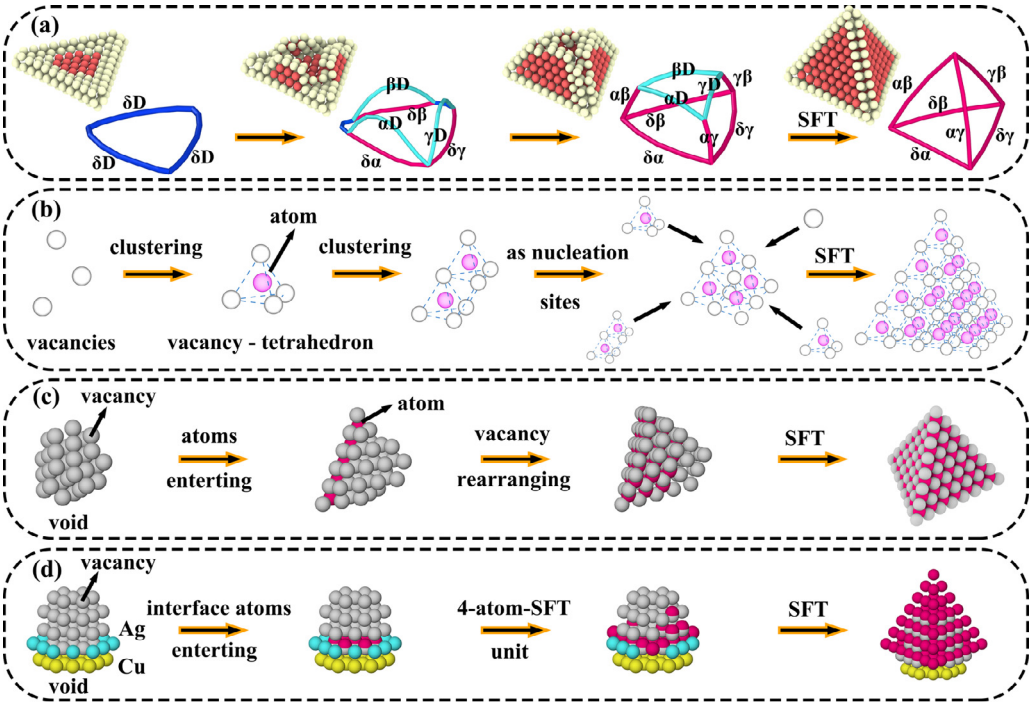

Fig. 9. Atomic-scale mechanisms for the formation of an SFT (a) through the dissociation of the Frank loop, (b) from vacancy and vacancy cluster aggregation, (c) from a void within a single crystal, and (d) through the sequential transformation from a void at a semi-coherent interface.

emit from the interface formed a defect rather than eliminating one. Many experimental and simulation studies [14–19] report that SFTs in the interior of the grain could be split or annihilated by interacting with gliding dislocations. Martínez and Uberuaga [71] also showed that small SFTs can diffuse by temporarily disrupting their structure through activated thermal events, and that the mobility of SFTs can be rather high, even higher than isolated vacancies. The present study further shows an interfacial effect that influences not only the void to SFT transformation, but also the initial growth of SFTs as well as their damage by interface dislocation nucleation.

Experimental studies have shown that a high density of bi-phase interfaces efficiently reduces irradiation defects or adjusts their distribution [26–32] and in efforts to design interfaces to optimize defect mitigation, studies on the mechanisms underlying defect/interface interactions can be useful. Based on our studies on Cu/Ag, we find that the distinct interface features that promote the void-to-SFT transformation are (i) the character of misfit dislocations; (ii) the non-uniform stress distribution; and (iii) the thermal fluctuation at relatively low temperature. Regarding (i) and (ii), the misfit dislocations forming between two dissimilar metals will generate atomically localized stress/strain fields that can reduce the activation barrier for the transformation at the interface. Such localized, non-uniform interface stresses drive the atom/vacancy in the defect cluster to hop, facilitating the transformation. This also brings into question the ability of other interfaces to facilitate the transformation. Recalling (i) and (ii), the character of the misfit dislocations determines the stress field they generate. Their characteristics are determined by the properties of the two adjoining materials, such as differences in their lattice constants, stacking fault energies (for fcc metals), and elastic moduli, and their orientation relationship, including crystal direction and crystal plane. For example, for the Ni/Ag interface [72] with the same orientation relationship, the lattice mismatch is 14.79%, which is larger than the 12.26% of the Cu/Ag interface. Thus, the Ni/Ag interface contains a higher density of the misfit dislocations and misfit dislocation intersections (MDIs), compared to the Cu/Ag interface. Moreover, the elastic modulus of Ni is higher than that of Cu, indicating that the Ni/Ag interface has a higher elastic mismatch than the Cu/Ag interface. For these reasons, it may be expected that the Ni/Ag interface is better able to promote the transformation. Yet, the misfit dislocation intersections (MDIs) of the Cu/Ni interface taken on a complex atomic structure in the form of a spiral, which leads to a highly non-local stress distribution in the interface [44]. Under these circumstances, which interface would better promote the transformation is not clear. Regarding fcc/bcc interfaces with a K-S orientation, such as Ag/V [73], Cu/V [74], Cu/Mo [75] and Cu/Nb [76], the misfit dislocation network adopts a block-like pattern, consisting of connected parallelograms. The spacings and Burgers vectors vary, however, among these Cu/V, Cu/Mo and Cu/Nb interfaces, leading to different capacities to trap He atoms at MDIs in interfaces, which can affect hardening [77]. For the void to SFT transformation process, these differences in the misfit dislocation network translate to differences in the local stress state, which would affect at the very least the first key hopping step that triggers the transformation. As demonstrated in Fig. 4, the energy barrier of the key step in the transformation is found to be much lower than that in the bulk. It should be noted that the stress field generated by the interfacial misfit dislocations can also play an important role in trapping vacancies, which are generated initially during irradiation [78,79]. A preferential drift of vacancies toward the interfaces is induced by this stress field [63–65,78], especially by the shear stress component [64]. Voids can also form at the interfaces by the aggregation of such vacancies, in addition to being created directly in the cascade process. Many of these characteristics are common to semi-coherent interfaces and some incoherent interfaces, suggesting that the mechanisms reported here can apply to other bimetallic systems. Regarding (iii), the present study demonstrates that a high temperature would accelerate the transformation from the void and bubble (with finite He concentrations) to the SFT.

5. Concluding remarks

In summary, we report an interface-facilitated mechanism for the direct transformation of a void (<2 nm diameter) into a stacking fault tetrahedron (SFT) in the FCC/FCC Cu/Ag system. Atomic-scale simulations

indicate that the non-uniform stress field that develops around the misfit dislocations at the semi-coherent interface can promote the direct transformation of a void into an SFT via a mechanism, which is different than that occurs in the single crystals. In the interface-facilitated transformation mechanism, vacancies initially jump at the relatively high atomic stress areas in the interface. The initial jump then triggers a series of vacancy jumps from the crystallographic layers adjacent to the interface. The bottom layer of the SFT first forms in the interface plane and grows. NEB calculations show that the activation energy barrier for the direct transformation at the interface has a much lower value than that associated with a similar void to SFT transformation in the single crystal. It is shown that compared to a pristine interface, SFT-containing interface can possess a much lower energy barrier for dislocation nucleation than a void-containing interface. The dislocation nucleation is more favorable in the former case when the newly emitted dislocations react with the SFT and damage it, enabling the interface to return to its planar, pristine state.

Declaration of Competing Interest

The authors declare that they have no known competing financial interests or personal relationships that could have appeared to influence the work reported in this paper.

Acknowledgments

This work is supported by National Key Research and Development Program of China (Nos. 2016YFC1102500 and 2017YFB0702100), National Natural Science Foundation of China (Project Nos. 51471018, 51672015, 51401208, 51771201, 11675230 and 11375242), and the “111 Project” (No. B17002). X.F.K. is supported by the Academic Excellence Foundation of BUAA for PhD Students. D.L. is supported by the European Regional Development Fund in the IT4Innovations National Supercomputing Center - Path to Exascale project, No. CZ.02.1.01/0.0/0.0/16_013/0001791 within the Operational Programme Research Development and Education and by SGS No. SP2020/150.

Supplementary materials

Supplementary material associated with this article can be found in the online version at doi:10.1016/j.actamat.2020.02.044.

References

[1] K. Niwase, F. Phillipp, W. Sigle, A. Seeger, Void formation close to stacking fault tetrahedra in heavily electron irradiated pure Ag and Cu, J. Nucl. Mater. 271–272 (1999) 261–265, doi: 10.1016/S0022-3115(98)00713-2.
[2] R. Schäublin, Z. Yao, N. Baluc, M. Victoria, Irradiation-induced stacking fault tetrahedra in fcc metals, Philos. Mag. 85 (2005) 769–777, doi: 10.1080/14786430412331319929.
[3] B.N. Singh, Effect of grain size on void formation during high-energy electron irradiation of austenitic stainless steel, Philos. Mag. 29 (1974) 25, doi: 10.1080/14786437408213551.
[4] K. Nordlund, F. Gao, Formation of stacking-fault tetrahedra in collision cascades, Appl. Phys. Lett. 74 (1999) 2720–2722, doi: 10.1063/1.123948.
[5] X. Zhang, K. Hattar, Y. Chen, L. Shao, J. Li, C. Sun, K. Yu, N. Li, M.L. Taheri, H. Wang, J. Wang, M. Nastasi, Radiation damage in nanostructured materials, Prog. Mater. Sci. 96 (2018) 217–321, doi: 10.1016/j.pmatsci.2018.03.002.
[6] S.J. Zinkle, K. Farrell, Void swelling and defect cluster formation in reactor-irradiated copper, J. Nucl. Mater. 168 (1989) 262–267, doi: 10.1016/0022-3115(89)90591-6.
[7] B.N. Singh, A. Horsewell, P. Toft, D.J. Edwards, Temperature and dose dependencies of microstructure and hardness of neutron irradiated OFHC copper, J. Nucl. Mater. 224 (1995) 131–140, doi: 10.1016/0022-3115(95)00054-2.
[8] M. Victoria, N. Baluc, C. Bailat, Y. Dai, M.I. Luppo, R. Schaublin, B.N. Singh, Microstructure and associated tensile properties of irradiated fcc and bcc metals, J. Nucl. Mater. 276 (2000) 114–122, doi: 10.1016/S0022-3115(99)00203-2.
[9] B.D. Wirth, How does radiation damage materials? Science (80-.) 318 (2007) 923–924 http://science.sciencemag.org/content/318/5852/923 .
[10] Y.N. Osetsky, D.J. Bacon, Atomic-Level interaction of an edge dislocation with localized obstacles in FCC and BCC metals, in: H. Kitagawa, Y. Shibutani (Eds.), IUTAM Symp. Mesoscopic Dyn. Fract. Process Mater. Strength, Springer Netherlands, Dordrecht, 2004, pp. 193–202.
[11] Y.N. Osetsky, D.J. Bacon, Atomic-scale mechanisms of void hardening in bcc and fcc metals, Philos. Mag. 90 (2010) 945–961, doi: 10.1080/14786430903164580.
[12] P. Grammatikopoulos, D.J. Bacon, Y.N. Osetsky, The influence of interaction geometry on the obstacle strength of voids and copper precipitates in iron, Model. Simul. Mater. Sci. Eng. 19 (2011) 015004, doi: 10.1088/0965-0393/19/1/015004.
[13] Y.N. Osetsky, D.J. Bacon, Atomic-level dislocation dynamics in irradiated metals, Compr. Nucl. Mater., Elsevier, 2012, pp. 333–356, doi: 10.1016/B978-0-08-056033-5.00028-8.
[14] Y. Matsukawa, S.J. Zinkle, Dynamic observation of the collapse process of a stacking fault tetrahedron by moving dislocations, J. Nucl. Mater. 329–333 (2004) 919–923, doi: 10.1016/j.jnucmat.2004.04.069.
[15] Y. Matsukawa, Y.N. Osetsky, R.E. Stoller, S.J. Zinkle, The collapse of stacking-fault tetrahedra by interaction with gliding dislocations, Mater. Sci. Eng. A 400–401 (2005) 366–369, doi: 10.1016/j.msea.2005.01.063.
[16] Y. Matsukawa, Y.N. Osetsky, R.E. Stoller, S.J. Zinkle, Destruction processes of large stacking fault tetrahedra induced by direct interaction with gliding dislocations, J. Nucl. Mater. 351 (2006) 285–294, doi: 10.1016/j.jnucmat.2006.02.003.
[17] Y.N. Osetsky, D. Rodney, D.J. Bacon, Atomic-scale study of dislocation–stacking fault tetrahedron interactions. Part I: mechanisms, Philos. Mag. 86 (2006) 2295–2313, doi: 10.1080/14786430500513783.
[18] J.S. Robach, I.M. Robertson, H.-J. Lee, B.D. Wirth, Dynamic observations and atomistic simulations of dislocation–defect interactions in rapidly quenched copper and gold, Acta Mater. 54 (2006) 1679–1690, doi: 10.1016/j.actamat.2005.11.038.
[19] M. Briceño, J. Kacher, I.M. Robertson, Dynamics of dislocation interactions with stacking-fault tetrahedra at high temperature, J. Nucl. Mater. 433 (2013) 390–396, doi: 10.1016/j.jnucmat.2012.10.004.
[20] Y.N. Osetsky, Y. Matsukawa, R.E. Stoller, S.J. Zinkle, On the features of dislocation-obstacle interaction in thin films: large-scale atomistic simulation, Philos. Mag. Lett. 86 (2006) 511–519, doi: 10.1080/09500830600908988.
[21] E. Martínez, A. Caro, I.J. Beyerlein, Atomistic modeling of defect-induced plasticity in CuNb nanocomposites, Phys. Rev. B. 90 (2014) 054103, doi: 10.1103/PhysRevB.90.054103.
[22] B.D. Wirth, V. Bulatov, T. Diaz de la Rubia, Atomistic simulation of stacking fault tetrahedra formation in Cu, J. Nucl. Mater. 283–287 (2000) 773–777, doi: 10.1016/S0022-3115(00)00262-2.
[23] J. Silcox, P.B. Hirsch, Direct observations of defects in quenched gold, Philos. Mag. 4 (1959) 72–89, doi: 10.1080/14786435908238228.
[24] L. Zhang, C. Lu, G. Michal, G. Deng, K. Tieu, The formation and destruction of stacking fault tetrahedron in fcc metals: a molecular dynamics study, Scr. Mater. 136 (2017) 78–82, doi: 10.1016/j.scriptamat.2017.04.019.
[25] B.P. Uberuaga, R.G. Hoagland, A.F. Voter, S.M. Valone, Direct transformation of vacancy voids to stacking fault tetrahedra, Phys. Rev. Lett. 99 (2007) 135501, doi: 10.1103/PhysRevLett.99.135501.
[26] K. Hattar, M.J. Demkowicz, A. Misra, I.M. Robertson, R.G. Hoagland, Arrest of He bubble growth in Cu-Nb multilayer nanocomposites, Scr. Mater. 58 (2008) 541–544, doi: 10.1016/j.scriptamat.2007.11.007.
[27] M.J. Demkowicz, R.G. Hoagland, J.P. Hirth, Interface structure and radiation damage resistance in Cu-Nb multilayer nanocomposites, Phys. Rev. Lett. 100 (2008) 2–5, doi: 10.1103/PhysRevLett.100.136102.
[28] X. Zhang, E.G. Fu, A. Misra, M.J. Demkowicz, Interface-enabled defect reduction in He ion irradiated metallic multilayers, JOM 62 (2010) 75–78, doi: 10.1007/s11837-010-0185-5.
[29] M.J. Demkowicz, D. Bhattacharyya, I. Usov, Y.Q. Wang, M. Nastasi, A. Misra, The effect of excess atomic volume on He bubble formation at fcc-bcc interfaces, Appl. Phys. Lett. 97 (2010) 1–4, doi: 10.1063/1.3502594.
[30] W. Han, M.J. Demkowicz, N.A. Mara, E. Fu, S. Sinha, A.D. Rollett, Y. Wang, J.S. Carpenter, I.J. Beyerlein, A. Misra, Design of radiation tolerant materials via interface engineering, Adv. Mater. 25 (2013) 6975–6979, doi: 10.1002/adma.201303400.
[31] I.J. Beyerlein, A. Caro, M.J. Demkowicz, N.A. Mara, A. Misra, B.P. Uberuaga, Radiation damage tolerant nanomaterials, Mater. Today 16 (2013) 443–449, doi: 10.1016/j.mattod.2013.10.019.
[32] E. Martínez, B.P. Uberuaga, I.J. Beyerlein, Interaction of small mobile stacking fault tetrahedra with free surfaces, dislocations, and interfaces in Cu and Cu-Nb, Phys. Rev. B 93 (2016) 054105, doi: 10.1103/PhysRevB.93.054105.
[33] L. Zhang, C. Lu, K. Tieu, L. Su, X. Zhao, L. Pei, Stacking fault tetrahedron induced plasticity in copper single crystal, Mater. Sci. Eng. A 680 (2017) 27–38, doi: 10.1016/j.msea.2016.10.034.
[34] H. Wang, D.S. Xu, R. Yang, P. Veyssire, The formation of stacking fault tetrahedra in Al and Cu: I. Dipole annihilation and the nucleation stage, Acta Mater. 59 (2011) 1–9, doi: 10.1016/j.actamat.2010.07.046.
[35] D.S. Aidhy, C. Lu, K. Jin, H. Bei, Y. Zhang, L. Wang, W.J. Weber, Formation and growth of stacking fault tetrahedra in Ni via vacancy aggregation mechanism, Scr. Mater. 114 (2016) 137–141, doi: 10.1016/j.scriptamat.2015.12.020.
[36] T.D. Shen, R.B. Schwarz, X. Zhang, Bulk nanostructured alloys prepared by flux melting and melt solidification, Appl. Phys. Lett. 87 (2005) 141906, doi: 10.1063/1.2056610.
[37] S. Plimpton, Fast parallel algorithms for short-range molecular dynamics, J. Comput. Phys. 117 (1995) 1–19, doi: 10.1006/jcph.1995.1039.
[38] Y. Mishin, M.J. Mehl, D.A. Papaconstantopoulos, A.F. Voter, J.D. Kress, Structural stability and lattice defects in copper: ab initio, tight-binding, and embedded-atom calculations, Phys. Rev. B 63 (2001) 224106, doi: 10.1103/PhysRevB.63.224106.

[39] P.L. Williams, Y. Mishin, J.C. Hamilton, An embedded-atom potential for the Cu–Ag system, Model. Simul. Mater. Sci. Eng. 14 (2006) 817–833, doi: 10.1088/0965-0393/14/5/002.
[40] H. Akbarzadeh, M. Mohammadzadeh, Adsorption of he gas on the AgN nanoclusters: a molecular dynamic study, Fluid Phase Equilib. 379 (2014) 175–179, doi: 10.1016/j.fluid.2014.07.028.
[41] W. Ling, N. Xi-Jing, Molecular dynamics simulations of helium behaviour in copper crystals, Chin. Phys. Lett. 20 (2003) 1416–1419, doi: 10.1088/0256-307X/20/9/302.
[42] S. Zheng, S. Shao, J. Zhang, Y. Wang, M.J. Demkowicz, I.J. Beyerlein, N.A. Mara, Adhesion of voids to bimetal interfaces with non-uniform energies, Sci. Rep. 5 (2015) 15428, doi: 10.1038/srep15428.
[43] J. Wang, R.G. Hoagland, J.P. Hirth, A. Misra, Atomistic simulations of the shear strength and sliding mechanisms of copper-niobium interfaces, Acta Mater. 56 (2008) 3109–3119, doi: 10.1016/j.actamat.2008.03.003.
[44] X.Y. Chen, X.F. Kong, A. Misra, D. Legut, B.N. Yao, T.C. Germann, R.F. Zhang, Effect of dynamic evolution of misfit dislocation pattern on dislocation nucleation and shear sliding at semi-coherent bimetal interfaces, Acta Mater. 143 (2018) 107–120, doi: 10.1016/j.actamat.2017.10.012.
[45] Y.Y. Xiao, X.F. Kong, B.N. Yao, D. Legut, T.C. Germann, R.F. Zhang, Atomistic insight into the dislocation nucleation at crystalline/crystalline and crystalline/amorphous interfaces without full symmetry, Acta Mater. 162 (2019) 255–267, doi: 10.1016/j.actamat.2018.09.068.
[46] X.F. Kong, I.J. Beyerlein, Z.R. Liu, B.N. Yao, D. Legut, T.C. Germann, R.F. Zhang, Stronger and more failure-resistant with three-dimensional serrated bimetal interfaces, Acta Mater. 166 (2019) 231–245, doi: 10.1016/j.actamat.2018.12.051.
[47] M. Wang, I.J. Beyerlein, J. Zhang, W. Han, Defect-interface interactions in irradiated Cu/Ag nanocomposites, Acta Mater. 160 (2018) 211–223, doi: 10.1016/j.actamat.2018.09.003.
[48] Y. Ding, J. Pencer, E. Torres, Atomistic simulation study of the helium effects on the deformation behavior in nickel bicrystals, J. Nucl. Mater. 516 (2019) 247–254, doi: 10.1016/j.jnucmat.2019.01.018.
[49] A. Stukowski, Visualization and analysis of atomistic simulation data with OVITO–the open visualization tool, Model. Simul. Mater. Sci. Eng. 18 (2010) 015012, doi: 10.1088/0965-0393/18/1/015012.
[50] K. Momma, F. Izumi, VESTA 3 for three-dimensional visualization of crystal, volumetric and morphology data, J. Appl. Crystallogr. 44 (2011) 1272–1276, doi: 10.1107/S0021889811038970.
[51] A. Stukowski, K. Albe, Extracting dislocations and non-dislocation crystal defects from atomistic simulation data, Model. Simul. Mater. Sci. Eng. (2010) 18, doi: 10.1088/0965-0393/18/8/085001.
[52] C.S. Hartley, Y. Mishin, Characterization and visualization of the lattice misfit associated with dislocation cores, Acta Mater. 53 (2005) 1313–1321, doi: 10.1016/j.actamat.2004.11.027.
[53] C.S. Hartley, Y. Mishin, Representation of dislocation cores using Nye tensor distributions, Mater. Sci. Eng. A 400–401 (2005) 18–21, doi: 10.1016/j.msea.2005.03.076.
[54] R.F. Zhang, B.N. Yao, AADIS: An atomistic analyzer for dislocation character and distribution, Comput. Phys. Commun. 247 (2020) 106857, doi: 10.1016/j.cpc.2019.07.020.
[55] F.Z. Dai, W.Z. Zhang, An automatic and simple method for specifying dislocation features in atomistic simulations, Comput. Phys. Commun. 188 (2015) 103–109, doi: 10.1016/j.cpc.2014.11.014.
[56] W. Han, E.G. Fu, M.J. Demkowicz, Y. Wang, A. Misra, Irradiation damage of single crystal, coarse-grained, and nanograined copper under helium bombardment at 450 °C, J. Mater. Res. 28 (2013) 2763–2770, doi: 10.1557/jmr.2013.283.
[57] W.Z. Han, M.J. Demkowicz, E.G. Fu, Y.Q. Wang, A. Misra, Effect of grain boundary character on sink efficiency, Acta Mater. 60 (2012) 6341–6351, doi: 10.1016/j.actamat.2012.08.009.
[58] R.F. Zhang, J. Wang, I.J. Beyerlein, A. Misra, T.C. Germann, Atomic-scale study of nucleation of dislocations from fcc-bcc interfaces, Acta Mater. 60 (2012) 2855–2865, doi: 10.1016/j.actamat.2012.01.050.
[59] A. Kashinath, A. Misra, M.J. Demkowicz, Stable storage of helium in nanoscale platelets at semicoherent interfaces, Phys. Rev. Lett. 110 (2013) 86101, doi: 10.1103/PhysRevLett.110.086101.
[60] Z. Di, X.-M. Bai, Q. Wei, J. Won, R.G. Hoagland, Y. Wang, A. Misra, B.P. Uberuaga, M. Nastasi, Tunable helium bubble superlattice ordered by screw dislocation network, Phys. Rev. B. 84 (2011) 052101, doi: 10.1103/PhysRevB.84.052101.
[61] W. Kurz, D.J. Fisher, Fundamentals of Solidification, fourth ed., Trans Tech Publications, Aedermannsdorf, Switzerland, 1998.
[62] G. Henkelman, H. Jónsson, Long time scale kinetic Monte Carlo simulations without lattice approximation and predefined event table, J. Chem. Phys. 115 (2001) 9657–9666, doi: 10.1063/1.1415500.
[63] K. Sato, T. Yoshiie, Y. Satoh, Q. Xu, M. Kiritani, Simulation of vacancy migration energy in Cu under high strain, Mater. Sci. Eng. A 350 (2003) 220–222, doi: 10.1016/S0921-5093(02)00692-5.
[64] J.-.W. Jang, J. Kwon, B.-J. Lee, Effect of stress on self-diffusion in bcc Fe: an atomistic simulation study, Scr. Mater. 63 (2010) 39–42, doi: 10.1016/j.scriptamat.2010.02.045.
[65] N. Gao, F. Gao, Z.-.G. Wang, Anisotropic migration of defects under strain effect in BCC iron, Chin. Phys. Lett. 34 (2017) 076102, doi: 10.1088/0256-307X/34/7/076102.
[66] J.B. Adams, W.G. Wolfer, Formation energies of helium-void complexes in nickel, J. Nucl. Mater. 166 (1989) 235–242, doi: 10.1016/0022-3115(89)90220-1.
[67] M. Wang, I.J. Beyerlein, J. Zhang, W. Han, Bi-metal interface-mediated defects distribution in neon ion bombarded Cu/Ag nanocomposites, Scr. Mater. 171 (2019) 1–5, doi: 10.1016/j.scriptamat.2019.06.016.
[68] S. Shao, J. Wang, I.J. Beyerlein, A. Misra, Glide dislocation nucleation from dislocation nodes at semi-coherent {1 1 1} Cu–Ni interfaces, Acta Mater. 98 (2015) 206–220, doi: 10.1016/j.actamat.2015.07.044.
[69] R. Li, H.B. Chew, Closed and open-ended stacking fault tetrahedra formation along the interfaces of Cu–Al nanolayered metals, Philos. Mag. 95 (2015) 2747–2763, doi: 10.1080/14786435.2015.1077283.
[70] H. Xiang, H. Li, T. Fu, W. Zhu, C. Huang, B. Yang, X. Peng, Shock-induced stacking fault pyramids in Ni/Al multilayers, Appl. Surf. Sci. 427 (2018) 219–225, doi: 10.1016/j.apsusc.2017.07.268.
[71] E. Martínez, B.P. Uberuaga, Mobility and coalescence of stacking fault tetrahedra in Cu, Sci. Rep. 5 (2015) 9084, doi: 10.1038/srep09084.
[72] K.Y. Yu, C. Sun, Y. Chen, Y. Liu, H. Wang, M.A. Kirk, M. Li, X. Zhang, Superior tolerance of Ag/Ni multilayers against Kr ion irradiation: an in situ study, Philos. Mag. 93 (2013) 3547–3562, doi: 10.1080/14786435.2013.815378.
[73] Q.M. Wei, N. Li, N. Mara, M. Nastasi, A. Misra, Suppression of irradiation hardening in nanoscale V/Ag multilayers, Acta Mater. 59 (2011) 6331–6340, doi: 10.1016/j.actamat.2011.06.043.
[74] S. Mao, S. Shu, J. Zhou, R.S. Averback, S.J. Dillon, Quantitative comparison of sink efficiency of Cu–Nb, Cu–V and Cu–Ni interfaces for point defects, Acta Mater. 82 (2015) 328–335, doi: 10.1016/j.actamat.2014.09.011.
[75] N. Li, J.J. Carter, A. Misra, L. Shao, H. Wang, X. Zhang, The influence of interfaces on the formation of bubbles in He-ion-irradiated Cu/Mo nanolayers, Philos. Mag. Lett. 91 (2011) 18–28, doi: 10.1080/09500839.2010.522210.
[76] W.Z. Han, E.K. Cerreta, N.A. Mara, I.J. Beyerlein, J.S. Carpenter, S.J. Zheng, C.P. Trujillo, P.O. Dickerson, A. Misra, Deformation and failure of shocked bulk Cu–Nb nanolaminates, Acta Mater. 63 (2014) 150–161, doi: 10.1016/j.actamat.2013.10.019.
[77] N. Li, M. Demkowicz, N. Mara, Y. Wang, A. Misra, Hardening due to interfacial He bubbles in nanolayered composites, Mater. Res. Lett. 4 (2016) 75–82, doi: 10.1080/21663831.2015.1110730.
[78] A. Vattré, T. Jourdan, H. Ding, M.-.C. Marinica, M.J. Demkowicz, Non-random walk diffusion enhances the sink strength of semicoherent interfaces, Nat. Commun. 7 (2016) 10424, doi: 10.1038/ncomms10424.
[79] M.J. Demkowicz, L. Thilly, Structure, shear resistance and interaction with point defects of interfaces in Cu-Nb nanocomposites synthesized by severe plastic deformation, Acta Mater. 59 (2011) 7744–7756, doi: 10.1016/j.actamat.2011.09.004.